JACS
JOURNAL OF THE AMERICAN CHEMICAL SOCIETY
Article
pubs.acs.org/JACS

Self-Assembly and Crystallization of Hairy (*f*-Star) and DNA-Grafted Nanocubes

Christopher Knorowski* and Alex Travesset

Department of Physics and Astronomy and Ames Laboratory, Iowa State University, Ames, Iowa 50011, United States

Supporting Information

ABSTRACT: Nanoparticle superlattices are key to realizing many of the materials that will solve current technological challenges. Particularly important for their optical, mechanical or catalytic properties are superlattices of anisotropic (non-spherical) nanoparticles. The key challenge is how to program anisotropic nanoparticles to self-assemble into the relevant structures. In this Article, using numerical simulations, we show that "hairy" (*f*-star) or DNA grafted on nanocubes provides a general framework to direct the self-assembly into phases with crystalline, liquid crystalline, rotator, or noncrystalline phases with both long-range positional and orientational order. We discuss the relevance of these phases for engineering nanomaterials or micromaterials displaying precise orientational order, realization of dry superlattices as well as for the field of programmed self-assembly of anisotropic nanoparticles in general.

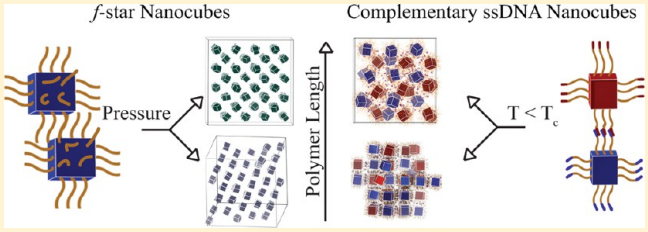

INTRODUCTION

Nanoparticle superlattices (NPS), arrangements of nanoparticles (NPs) into periodic structures, have direct applications for novel fuel cell membranes, solar photovoltaics, carbon dioxide storage, or catalytic materials among many others. The optimal strategy to engineer NPS is self-assembly, where the different components spontaneously assemble into the desired material. Yet, direct self-assembly of NPs into NPS is considerably difficult, as it only succeeds under very precise environmental conditions.[1−5] An alternative elegant route is to program self-assembly by controlling NPs interactions through a linker molecule such as DNA.[6,7] Over the past few years, DNA programmed self-assembly has proven to be an extremely versatile and general strategy to engineer NPS.[8−11]

Systems of spherical NPs with isotropically distributed DNA strands have been widely studied and exhibit a very rich phase diagram,[11] yet, many of the relevant NPS required in applications can only be self-assembled if the components (the NPs) display some degree of anisotropy. Precision NP synthesis provides different ways of inducing NP anisotropy, such as geometry (or shape), patchiness, etc.[12] DNA programmed self-assembly of NPs with different shapes such as rods, prism, triangles, octahedra, and dodecahedra have shown typical anisotropic NPS such as hexagonal and lamellar[10] as well as linear mesostructures.[13]

In this paper, we provide a characterization of the phase diagram and the dynamics of nanocubes (NCs), one of the simplest anisotropic nanoparticles, with attached ssDNA strands. We consider hard cubes, the case of ssDNA without complementary base pairs (an *f*-star polymer system) and with complementary strands (standard hybridization), as shown in Figure 1. The studies will be entirely conducted by the model previously developed by our group:[14] Because of its success in predicting equilibrium phases for spherical NPs, both for equal radii[14] as well as different radii,[15,16] 1D structures of triangular prisms[17] and the dynamics of self-assembly,[16,18] in all cases with nearly perfect agreement with experiments and without fitting parameters, the model has earned an obvious status as a very

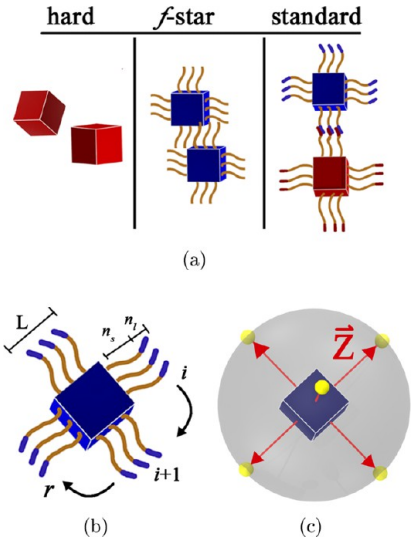

Figure 1. (a) Representation of the three NC systems studied in this paper: hard, *f*-star, and standard hybridization. (b) Cartoon of NC showing parameters L, n_s, n_l, r, and normal vector $\vec{Z}$. (c) Example Gauss map for a single NC showing normal vectors of a cube mapped onto a sphere S^2.

Received: June 20, 2013
Published: December 10, 2013

   dx.doi.org/10.1021/ja406241n | J. Am. Chem. Soc. 2014, 136, 653−659

rigorous and faithful representation of the actual experimental system.

All previous studies dealing with NC have focused on the simple case of hard cubes (see Figure 1), where the phase diagram is a function of the packing fraction only. Monte Carlo calculations determined a liquid and solid simple cubic (sc) crystal for small and close to one packing fractions respectively, separated by an intermediate cubatic phase.[19,20] Recent studies,[21] however, have disputed the existence of the cubatic phase and proposed a crystalline phase with a high vacancy density instead. Experimental models of hard cubes exist, in NCs[22] as well as colloidal-sized cubes,[23] and have revealed both the liquid and the sc crystal. Somewhat more complex systems consisting of cubes under variable surfactant coverings,[24] show a continuous transformation from a sc (at zero covering) to fcc (at maximum covering), which has been interpreted in terms of packings of "superballs",[25] intermediate shapes between cubes and spheres. Yet, the experimentally relevant case of nanocubes grafted with polymers, the subject of this paper, has remained a completely unexplored problem, despite its obvious implications for the engineering of new materials.

METHODS

We consider cubes that are L beads long, where each bead has diameter $\sigma \approx 2$ nm.[14] Each cube contains r ssDNA, and each strand consists of n_t flexible monomers of diameter σ. In the standard hybridization case, the n_t monomers consist of n_s spacers and n_l linkers, with $n_t = n_s + n_l$, while for the f-star case $n_t = n_s$ (see Figure 1). The parameters describing the system are the packing fraction ϕ, the grafting density ν, and the fractional polymer length λ, defined as

$$\begin{aligned} \phi &= \frac{N(L^3 + \pi n_t r/6)\sigma^3}{V} \\ \nu &= \frac{r}{6}\frac{1}{L^2} \\ \lambda &= \frac{n_t}{L} \end{aligned} \tag{1}$$

where V is the volume of the system and N the number of NCs. For simplicity, and consistently with previous studies, the number of linkers will be fixed to $n_l = 3$.[14,18] In the standard hybridization case, half of the NCs ($N/2$) have complementary linker ssDNA strands to the other half. For comparison with experiments, $L = 6$ and 9 corresponds to physical NC lengths of 12 and 18 nm, respectively, and the simulations cover ssDNA in the $n_s = 5-50$ base pair (bp) range and $n_l = 20$ bp.

Simulations were carried out under both the NPE ensemble using the Berendsen thermostat and NVT ensembles using the Nosé-Hoover thermostat, with some refinements discussed below. The time step was $\delta t = 0.005$ (simulation units of $(m\sigma^2/\epsilon)^{1/2}$) and simulations used the HOOMD blue software package (highly optimized object-oriented many particle dynamics), a highly parallelized version of MD designed to run entirely on GPUs.[26,27] The beads on each NC are held together by rigid body dynamics.[28] Because the model is the same as the one used in previous studies, we refer to the original references[14,18] for further technical details. Initial configurations are randomly generated using packmol.[29] Visual inspection and analysis were carried out using vmd.[30] Extensive simulations were done for system sizes $N = 54-128$. In some cases, finite size effects were assessed by running larger systems of up to $N = 256$ and 512 NPs.

Phases of NCs may exhibit orientational (liquid crystalline) or positional (plastic/rotator) order or both. Positional order is characterized from the local bond order parameters,[31] which allows identification of solid particles with a particular symmetry. The total number of solid particles thus extracted is presented as the fraction of solid particles within the system f_n(solid), where $n = 4$, 6, are sensitive to four-fold or six-fold symmetries. Additional characterization of positional order is provided by the static structure factor $S(\vec{q})$ and the radial distribution function $g(\vec{r})$, as used in previous studies.[14,18,32] The number of configurations of a cube with six indistinguishable faces is the same as the elements of the manifold defined by $SO(3)/O_h$, where O_h is the 48 element point group defining the cube isometries, thus, a convenient order parameter is

$$Q^{l}_{\alpha\beta} = \frac{1}{N}\sum_{i=1}^{N}\left\langle (\vec{Z}_i^{\nu_l})_\alpha (\vec{Z}_i^{\nu_l})_\beta \right\rangle - M_{\alpha\beta} \equiv N^{l}_{\alpha\beta} - M_{\alpha\beta} \tag{2}$$

where $\vec{Z}_i^{\mu}$ are the normal vectors to each of the six NC faces ($\mu = 1-6$) and $i = 1, ..., N$ runs through each NC on the system (Figure 1). The index ν_l indicates that only the NC normal closest to the direction defined by the fixed vector $\vec{w}_l$ in the laboratory frame is included in the average. The elements of the matrix $M_{\alpha\beta}$ and a more detailed discussion are provided in Supporting Information S1 and S2. The order parameter thus defined is such that $Q^{l}_{\alpha\beta} \neq 0$ if there is orientational order. In this case, the three $N^{l}_{\alpha\beta}$ eigenvalues identify the different phases, and in figures they are displayed as an order parameter defined in Supporting Information S7.

A complementary way to characterize orientational order is through a Gauss map (see Figure 2, where each of the six normals of every cube is mapped into the sphere S^2, see Figure 1c) In this paper, only four types of orientational order need to be considered: isotropic (I), C, anti-C (A), and Bakos (B). The Gauss map for each case is shown in Figure 2, and the eigenvalues of the $N^{l}_{\alpha\beta}$ are provided in Supporting Information S7.

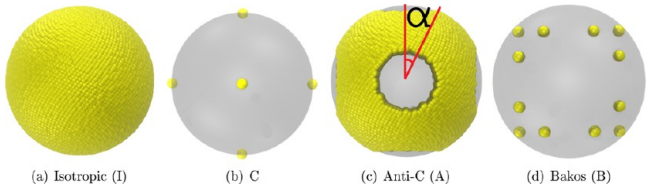

Figure 2. Gauss map of the four types of orientational order considered in this paper. Yellow dots represent the positions of cube normals. α is the size of the aperture angle.

The rotational dynamics are characterized from the rotational diffusion coefficient, D_a, defined as

$$\frac{1}{N}\sum_{i=1}^{N}\langle \vec{Z}_i^{\alpha}(t_0)\cdot\vec{Z}_i^{\alpha}(t)\rangle = e^{-2D_a(t-t_0)} \tag{3}$$

where α represents a preselected normal to the cube that is followed over time.

We label the different phases by its orientational and positional order. In addition, within standard hybridization, NCs with the same ssDNA sequence may display long-range positional order, which herein we denote as AB order. The standard CsCl-bcc found with spherical NPs[8,9] is an example of AB order. If such order is not present, it is denoted as D (disordered). The phases are labeled according to the convention:

AB or D orientational order−positional order

Thus, in an AB A-bcc phase, NCs display Anti-C orientational order and bcc positional order. For f-star systems, the prefix AB/D is meaningless, as all NCs are identical. It should be noted that, despite exhibiting both long-range positional and orientational order, phases are not necessarily crystalline, as there may not be a unit cell from which the lattice may be constructed by translations.

RESULTS AND DISCUSSION

***f*-Star NCs.** The phase diagram for f-star NCs was obtained from compression and expansion runs, similarly as in ref 19, but with some important modifications as compression rates were adjusted at the liquid-to-solid transition. The resulting phase

dx.doi.org/10.1021/ja406241n | J. Am. Chem. Soc. 2014, 136, 653−659

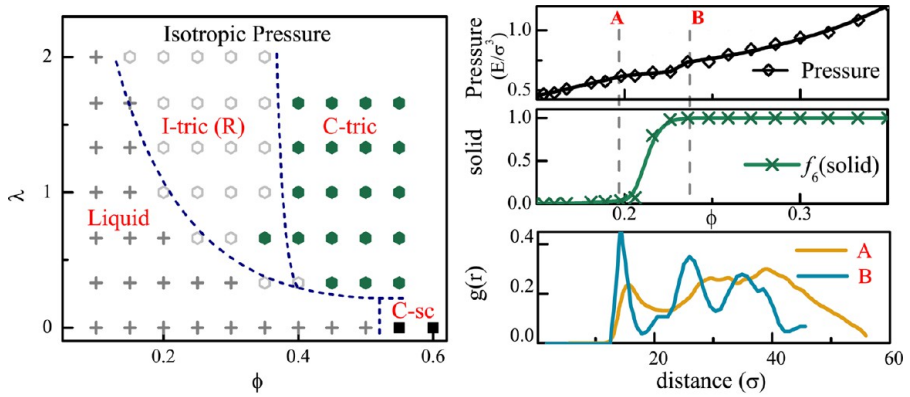

Figure 3. (a) Phase diagram for *f*-star NCs as a function of λ and ϕ (defined in eq 1) for isotropic pressure. (b) Equation of state (top) and fraction of solid particles (middle) as a function of packing fraction, ϕ, for a system of NCs, λ = 0.66, during the transition from liquid C-tric under compression. (Bottom) $g(r)$ for the liquid and crystal at points A and B before and after the disorder−order transition. All lines are drawn to guide the eye.

diagrams were obtained by repeating entire compression runs many times and using different compression rates as well as cycles over compression and expansion runs to ensure that the process was quasistatic and represented a succession of equilibrium states.

The resulting phase diagram is shown in Figure 3 for isotropic pressure for system sizes ranging from 54 to 1400 NCs. The case λ = 0 corresponds to hard cubes and includes an I-Liquid and a C-sc phase only (see snapshot in Figure 5). As a function of λ the C-sc phase becomes unstable, being replaced by a triclinic (tric) phase (snapshots in Figure 5), first as an I-tric(R), which converges to C-tric at higher packing densities. The equation of state is shown in Figure 3b as a function of packing fraction ϕ. There is a small change in slope of the equation of state when there is coexistence as clusters of solid particles begin to nucleate from the liquid (Figure 3b, middle), and a discontinuity in the equation of state at the disorder−order transition. Discrimination between the disorder and order transition is provided by the $g(r)$ (Figure 3b, bottom), which shows a disordered distribution for the liquid and distinct peaks for the ordered structure in I-tric(R). A snapshot of a C-tric phase for N = 512 NC and λ = 0.66 is shown in Figure 4. Two

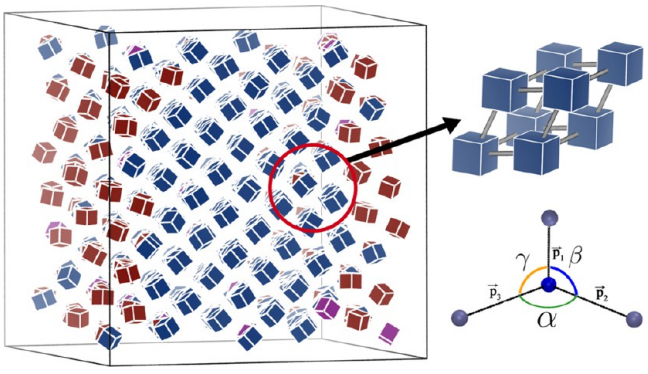

Figure 4. Snapshot of *f*-star C-tric at λ = 0.66 and packing fraction ϕ = 0.45 for isotropic pressure. There are two orientational domains found within the crystal, drawn as blue and red. Purple cubes are part of defects which do not follow the red or blue domains. The polymer is hidden for clarity. (Top right) Unit cell for C-tric showing blue cube orientation. (Bottom right) Definition of the primitive vectors.

different orientational domains can be seen in the system, denoted by red and blue colors. The unit cell for the C-tric is drawn in Figure 4, where angles $\alpha \neq \beta \neq \gamma$. It was found that the angles α, β, and γ did not significantly change as a function of packing fraction, ϕ, but did show considerable variation as a function of polymer length λ. As λ grows larger, the triclinic unit cell approaches the bcc limit seen in spherical NPs.[14] Explicit results are provided in Supporting Information S8.

Within the NVT ensemble, compression runs may result in anisotropic pressures $p_{xx} \neq p_{yy} \neq p_{zz}$ with off-diagonal terms being zero. For the case of high anisotropic pressure, the phase diagram shows surprising new phases (Figure 6a). For small λ a B-bcc phase is formed, where each NC is oriented in one of the four discrete orientations that define the Bakos four-cube compound,[33] see snapshots and Gauss map in Figure 5 (see also Supporting Information S4 and S5). As λ is increased to $\gtrsim$1, the B-bcc phase is replaced by an A-bcc (Anti-C) phase, where cube orientations on a cone of aperture angle α around the six orientations defined by C orientational order are not allowed; see Figure 5 for snapshot and the ideal Gauss map in Figure 2. The typical anisotropic pressures that develop in the A-bcc (R) and B-bcc are shown in Figure 6b.

Phases with anisotropic pressure are only found in simulations with up to 128 NCs, but we note that we did not attempt to simulate larger systems (using the NPE ensemble with Berendsen thermostat) as it is technically challenging to stabilize large anisotropic pressures. However, because we repeatedly obtained such phases regardless of compression rates, these phases are stable and not an artifact of the boundary conditions.

The rotational diffusion coefficients D_a (defined in eq 3) are plotted in Figure 7. It is clear that the NCs rotate considerably, and this is denoted with (R), rotator phases, in the phase diagram Figures 3 and 6. The variations of f_6, f_4, D_a, and $Q_{\alpha\beta}$ as functions of packing fraction are shown in Figure 7. The hard NCs systems show a transition from an I-liquid to a C-sc with no evidence for an intermediate liquid crystalline cubatic phase within ϕ = 0.52−0.56 (Figure 3), in disagreement with[19,20] but consistent with the presence of vacancies recently reported in ref 21, although the system sizes investigated are smaller.

We find that there is significant competition between orientational and positional order in these systems. The system either has bcc positional order which allows for four

dx.doi.org/10.1021/ja406241n | J. Am. Chem. Soc. 2014, 136, 653−659

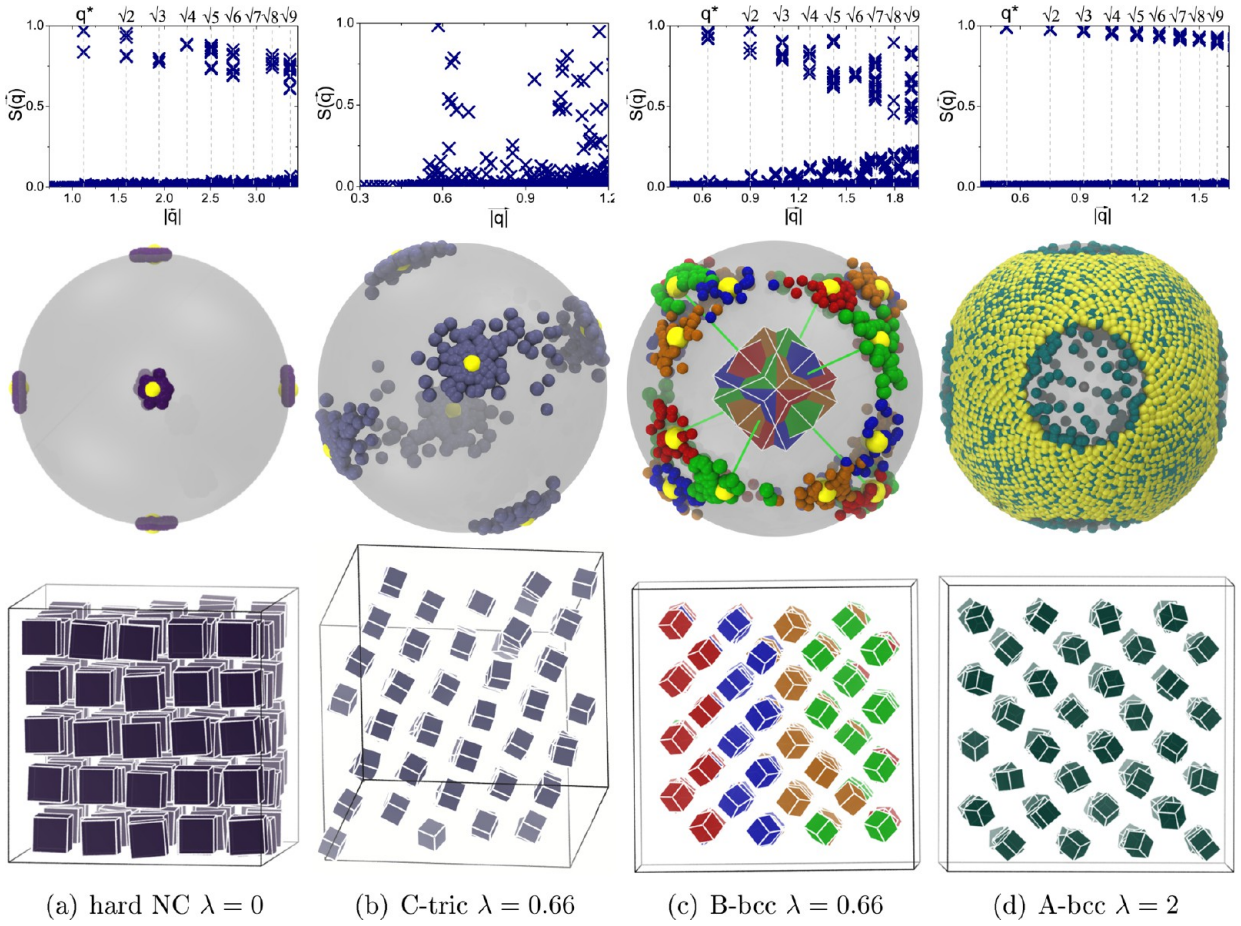

Figure 5. Phases for hard NC C-sc (a), and *f*-star system, C-tric (b) and B-bcc (c) and A-bcc(d), as a function λ (fractional polymer length) at high grafting density $\nu = 0.65$ (see eq 1 for parameter definitions). (Top) Structure factors, $S(\vec{q})$, with bcc peaks labeled. (Middle) Gauss map showing the normals of each NC mapped on to a sphere. Yellow beads in Gauss map are the ideal case (see 2). (bottom) Snapshots of each phase with the polymer removed in b–d for ease of viewing. Colors of NCs correspond to cube orientations as identified in the Gauss maps (middle).

orientations of NCs or a distortion of the bcc which favors a single orientation. Systems with triclinic positional order tend to have C orientational order, as the triclinic positional order breaks the orientational symmetry allowing a single preferential orientation of NCs to dominate. Defects such as interstitials in the system can have a large effect on orientation ordering making crystals with single orientations difficult to achieve (Figure 4). The length of the polymer will also have an effect on the degree to which the system is triclinic. While the system approaches bcc limit for increasing value of λ, our results clearly suggest that it does so through an intermediate orthorhombic lattice, as shown in Supporting Information S8.

Standard Hybridization of NCs. The case of standard hybridization, where DNA linkers are able to hybridize presents considerable challenges. As previously found, spherical NPs above the DNA melting temperature, T_c, become equivalent to an *f*-star system, while it is only for temperatures just slightly below T_c that the system may equilibrate within available simulation time.[14] Constant temperature MD becomes very challenging because of the slow rotational diffusion of NCs. For this reason, all MD runs were started with a random configuration at $T > T_c$, subsequently annealed to the target temperature $T < T_c$. Typical examples of annealing runs are shown in Figure 8.

The phase diagram depends on T as well as the three parameters ϕ, ν, and λ defined in eq 1. To reach a greater range for the values of λ the phase diagram for NC of length $L = 12$ and 18 nm was obtained as a function of T (see Figure 9), which is consistent for both NC sizes. Long-range order was obtained for grafting densities $\nu \gtrsim 0.25$, so we will present results for $\nu = 0.25$. The phase diagram as a function of T and λ is shown in Figure 10. For $T > T_c$ the system is equivalent to a *f*-star system, and the same D I-bcc phase of Figure 6 is obtained. Below T_c, the system aggregates into condensed phases, which are AB C-sc and AB I-bcc phases, with typical snapshots shown in Figure 8.

These results show how DNA hybridization can be used to control orientational order. For short DNA, $\lambda < 1$, NCs orient face to face, forming a C-sc superlattice, but, as the DNA strands are increased in length, NCs become isotropically distributed, akin to an *orientational glass*. Additionally, studies of DNA-hybridized 1D prisms[17] have shown a similar relationship between orientational order and DNA length, suggesting that face to face ordering for $\lambda < 1$ may be general result for other geometries as well.

The connection between the phases of *f*-star systems and standard hybridization becomes even more clear by subjecting the latter to finite osmotic pressure, by slowly compressing the system right below T_c. Starting with AB I-bcc phases, the phase diagram as a function of osmotic pressure (or packing fraction) becomes basically equivalent to the one obtained for *f*-star polymers (Figure 6 for anisotropic pressure), despite the

dx.doi.org/10.1021/ja406241n | J. Am. Chem. Soc. 2014, 136, 653–659

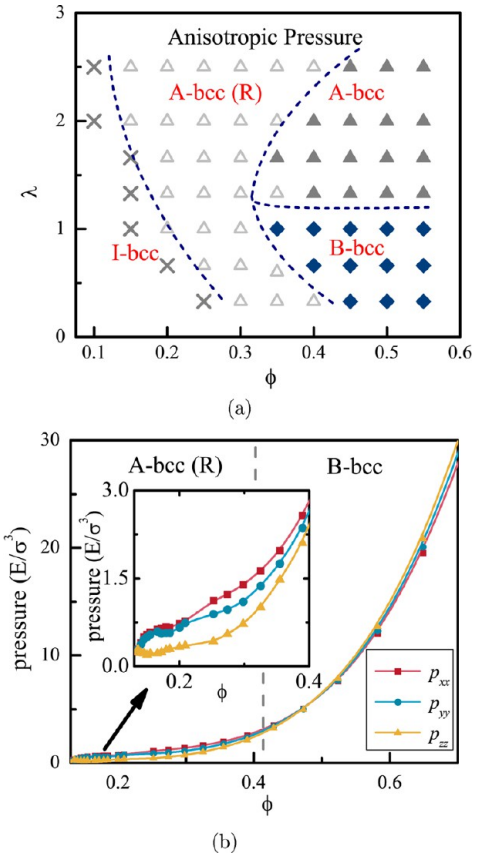

Figure 6. (a) Phase diagram *f*-star NCs as a function of λ and packing fraction, ϕ, for anisotropic pressures. (b) Equation of state showing p_{xx}, p_{yy}, and p_{zz} for a system of $N = 128$, $\lambda = 1$ which forms B-bcc under compression. Approximate ratios of pressure for A-bcc (R) are p_{xx}:p_{yy} = 1.1, p_{xx}:p_{zz} = 2.25, and for B-bcc are p_{xx}:p_{yy} = 0.96, p_{xx}:p_{zz} = 0.92.

pressure being isotropic for ssDNA hybridized phases. An equilibrated AB A-bcc phase under compression is shown in Figure 10.

CONCLUSION

In this paper we have provided, for the first time, the characterization of the phase diagram for cubes with grafted polymers ("hairy" or *f*-star systems) as well as with hybridizable DNA linkers. The results for *f*-star systems show a phase diagram with triclinic unit cells. The triclinic unit cell interpolates in between sc(hard cubes, zero polymer length) and bcc(long polymers described by spherical *f*-star systems), similarly as cuboid systems interpolate between sc and fcc[24,25] For significantly anisotropic osmotic pressures, the system exhibits a perfect bcc (cubic space group) but with complex orientational order (A or B, see Figure 5). Our results show that the geometric frustration induced by the polymer generates a competition between orientational order and a loss of cubic symmetry against a loss of orientation order and cubic symmetry; it is not possible to have both orientaional order and cubic symmetry, as is the case for hard cubes, since this situation is inefficient in accommodating the grafted polymer within the unit cell. As a result of the geometric frustration induced by the polymer, a more detailed study may reveal a finer additional structure beyond that predicted in this paper.

Our study of NCs provides the first characterization of DNA programmed self-assembly with anisotropic (nonspherical)

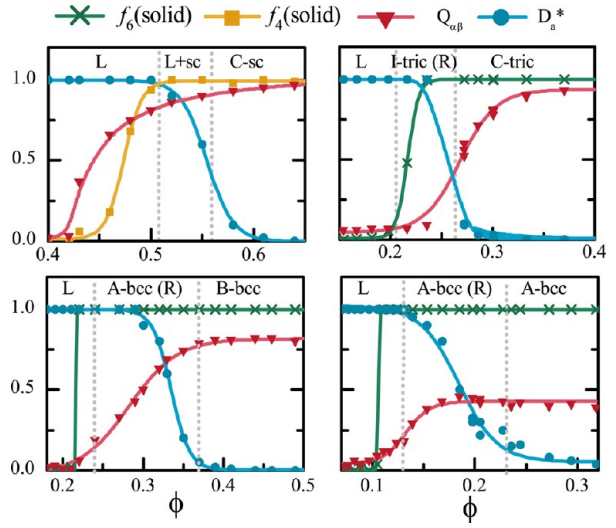

Figure 7. Compression runs for hard NCs ($N = 125$) (top left) and *f*-star polymers systems ($N = 128$, $\nu = 0.65$): $\lambda = 0.66$ (top right), 0.66 (bottom left), and 2.0 (bottom right). The percentage of solid particles defined by local bond ordering with bcc and tric, f_6(solid), as well as sc, *f*4(solid), positional order are plotted in green and yellow, respectively. The normalized rotational diffusion coefficient, D_a*, is plotted where unity is the resolution of our simulation time step. The orientational order parameter, $Q_{\alpha\beta}$, is plotted as well with respect to the vector which maximizes $Q_{\alpha\beta}$ for each system (see Supporting Information S4–S7). All lines are drawn to help guide the eye.

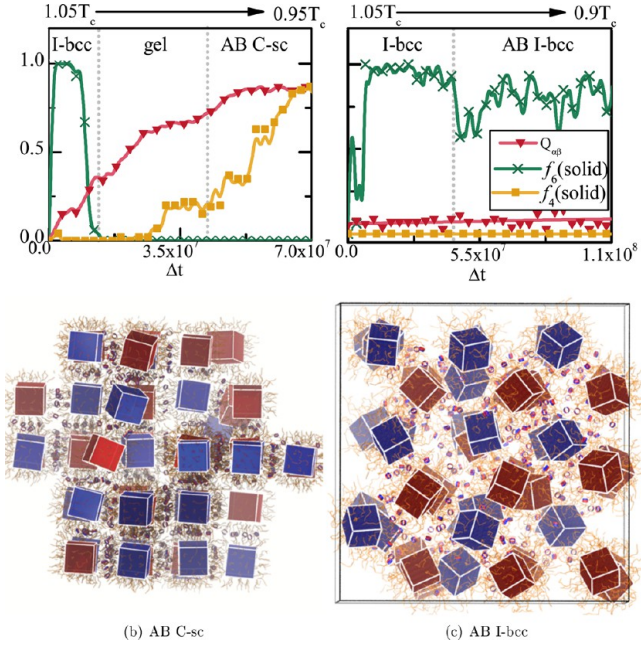

Figure 8. (Top) Dynamics for standard hybridization for simulations starting from a random configuration above T_c and cooling: (top left) $\lambda = 0.44$, $\nu = 0.25$; (top right) $\lambda = 2$, $\nu = 0.25$. (Bottom) Snapshots of the phases AB C-sc and AB I-bcc obtained. DNA is drawn in orange, and hybridization locations are marked as rings. Type A/B NCs are drawn in red/blue.

NPs. Our results show that for short DNA strands, the phase diagram consists of NCs that hybridize face to face, resulting in sc lattices. As the DNA becomes longer, the bcc phase of spherical systems is obtained. At finite osmotic pressures, a more complex phase diagram, with phases that reproduce those

dx.doi.org/10.1021/ja406241n | J. Am. Chem. Soc. 2014, 136, 653–659

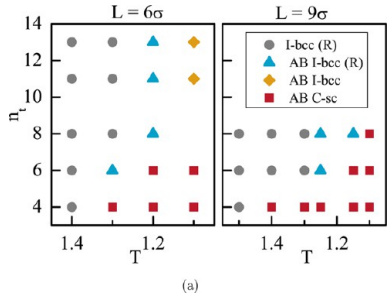

Figure 9. Phase diagram of standard hybridization as a function of n_t and T_c for $L = 6\sigma$ and $L = 9\sigma$ NCs. The packing fraction is determined from the I-bcc phase separately for each n_t.

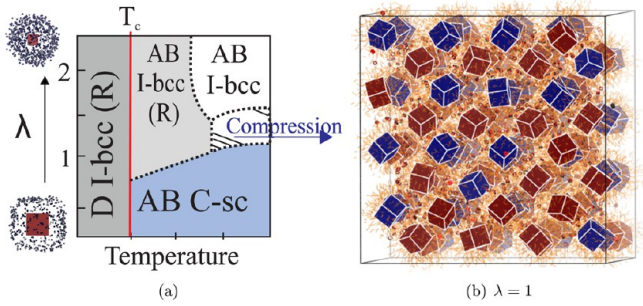

Figure 10. (a) Generalized phase diagram of standard hybridization as a function of λ and T. (b) Snapshot of an AB A-bcc phase obtained at finite osmotic pressure by compressing an AB I-bcc (R) ($\lambda = 1.33$, $L = 6\sigma$).

of the *f*-star NCs, but with additional type order (AB), are predicted.

The significance of our results extends beyond nanoscience, as *f*-star systems of colloidal size can be easily realized by grafting polymers to cubes with desired grafting densities ν and fractional polymer lengths λ, with the packing fraction being controlled by the same techniques used by Rossi et al.[23] for hard cubes. Yet, unlike the case of hard cubes, the presence of a polymer shell allows for UV polymerization and the ability to synthesize dry materials. Alternative routes are provided by plasma polymerization techniques,[35] which allow replacing the polymer by inorganic components. In this way, our predicted phases for *f*-star polymers provide a strategy to design new materials consisting of cubes where the orientations can be exquisitely adjusted.

The results in this paper have important implications for the DNA programmed self-assembly of NCs and other anisotropic NPs. Our results predict that for relatively short DNA strands, NCs are oriented face to face, but many other superlattices can be obtained by subjecting the system to an external osmotic pressure. It is not difficult to control osmotic pressure in nanoscale systems, as existing techniques are available.[36] There are also different strategies that allow transferring those materials to dry conditions.

Probably, the main difficulty for experiments with NCs are the sluggish dynamics resulting from rotational diffusion and the annihilation of topological defects. This is a particularly important subject for growing the type of high-quality crystals obtained with spherical NPs.[18] A detailed description of the dynamics of self-assembly is left for future work.

■ ASSOCIATED CONTENT

Supporting Information

Details of the orientational order parameters used to identify the different types of orientational order presented in this paper, simulation results for the unit cell of the C-tric phase as a function of λ, and details for unit cell analysis. This material is available free of charge via the Internet at http://pubs.acs.org.

■ AUTHOR INFORMATION

Corresponding Author

cdknorow@iastate.edu

Notes

The authors declare no competing financial interest.

■ ACKNOWLEDGMENTS

We acknowledge discussions and interest with R. Kamien and O. Gang. We also thank J. Anderson for help with HOOMD-blue as well as Martin Bertrand for help with the Berendsen thermostat. This work is funded by the U.S. DOE through the Ames Laboratory under Contract DE-AC02-07CH11358.

■ REFERENCES

(1) Kiely, C. J.; Fink, J.; Brust, M.; Bethell, D.; Schiffrin, D. J. *Nature* **1998**, *396*, 444.
(2) Wong, S.; Kitaev, V.; Ozin, G. *J. Am. Chem. Soc.* **2003**, *125*, 15589.
(3) Kalsin, A. M.; Fialkowski, M.; Paszewski, M.; Smoukov, S. K.; Bishop, K. J. M.; Grzybowski, B. A. *Science* **2006**, *312*, 420.
(4) Shevchenko, E. V.; Talapin, D. V.; Kotov, N. A.; O'Brien, S.; Murray, C. B. *Nature* **2006**, *439*, 55.
(5) Zheng, J.; Constantinou, P. E.; Micheel, C.; Alivisatos, A. P.; Kiehl, R. A.; Seeman, N. C. *Nano Lett.* **2006**, *6*, 1502.
(6) Mirkin, C. A.; Letsinger, R. L.; Mucic, R. C.; Storhoff, J. J. *Nature* **1996**, *382*, 607.
(7) Alivisatos, A. P.; Johnsson, K. P.; Peng, X.; Wilson, T. E.; Loweth, C. J.; Bruchez, M. P.; Schultz, P. G. *Nature* **1996**, *382*, 609.
(8) Park, S. Y.; Lytton-Jean, A. K. R.; Lee, B.; Weigand, S.; Schatz, G. C.; Mirkin, C. A. *Nature* **2008**, *451*, 553.
(9) Nykypanchuk, D.; Maye, M. M.; van der Lelie, D.; Gang, O. *Nature* **2008**, *451*, 549.
(10) Jones, M. R.; Macfarlane, R. J.; Lee, B.; Zhang, J.; Young, K. L.; Senesi, A. J.; Mirkin, C. A. *Nat. Mater.* **2010**, *9*, 913.
(11) Macfarlane, R. J.; Lee, B.; Jones, M. R.; Harris, N.; Schatz, G. C.; Mirkin, C. A. *Science* **2011**, *334*, 204.
(12) Glotzer, S. C.; Solomon, M. J. *Nat. Mater.* **2007**, *6*, 557.
(13) Vial, S.; Nykypanchuk, D.; Yager, K.; Tkachenko, A.; Gang, O. *ACS Nano* **2013**, *7*, 5437.
(14) Knorowski, C.; Burleigh, S.; Travesset, A. *Phys. Rev. Lett.* **2011**, *106*, 215501.
(15) Li, T.; Sknepnek, R.; Macfarlane, R. J.; Mirkin, C. A.; Olvera de la Cruz, M. *Nano Lett.* **2012**, *12*, 2509.
(16) Li, T.; Sknepnek, R.; Olvera de la Cruz, M. *J. Am. Chem. Soc.* **2013**, *135*, 8535.
(17) Kohlstedt, L.; Olvera de la Cruz, M.; Schatz, G. *J. Phys. Chem. Lett.* **2012**, *4*, 203.
(18) Knorowski, C.; Travesset, A. *Soft Matter* **2012**, *8*, 12053.
(19) John, B.; Stroock, A.; Escobedo, F. *J. Chem. Phys.* **2004**, *120*, 9383.
(20) Agarwal, U.; Escobedo, F. *Nat. Mater.* **2011**, *10*, 230.
(21) Smallenburg, F.; Filion, L.; Marechal, M.; Dijkstra, M. *Proc. Natl. Acad. Sci. U.S.A.* **2012**, *109*, 17886.
(22) Yamamuro, S.; Sumiyama, K.; Kamiyama, T. *Appl. Phys. Lett.* **2008**, *92*, 113108.
(23) Rossi, L.; Sacanna, S.; Irvine, W. T. M.; Chaikin, P. M.; Pine, D. J.; Philipse, A. P. *Soft Matter* **2011**, *7*, 4139.

(24) Zhang, Y.; Lu, F.; van der Lelie, D.; Gang, O. *Phys. Rev. Lett.* **2011**, *107*, 135701.
(25) Jiao, Y.; Stillinger, F.; Torquato, S. *Phys. Rev. E* **2009**, *79*, 041309.
(26) Anderson, J.; Lorenz, C.; Travesset, A. *J. Comput. Phys.* **2008**, *227*, 5342.
(27) http://codeblue.umich.edu/hoomd-blue/
(28) Nguyen, T.; Phillips, C.; Anderson, J. A.; Glotzer, S. C. *Comput. Phys. Commun.* **2011**, *182*, 2307.
(29) Martinez, L.; Andrade, R.; Birgin, E. G.; Martinez, J. M. *J. Comput. Chem.* **2009**, *30*, 2157.
(30) Humphrey, W.; Dalke, A.; Schulten, K. *J. Mol. Graphics* **1996**, *14*, 33.
(31) Steinhardt, P.; Nelson, D.; Ronchetti, M. *Phys. Rev. B* **1983**, *28*, 784.
(32) Knorowski, C.; Travesset, A. *Curr. Opin. Solid State Mater. Sci.* **2011**, *15*, 262.
(33) Bakos, T. *Math. Gazz.* **1959**, *43*, 17.
(34) Watzlawek, M.; Likos, C.; Lowen, H. *Phys. Rev. Lett.* **1999**, *82*, 5289.
(35) Cademartiri, L.; Ghadimi, A.; Ozin, G. *Acc. Chem. Res.* **2008**, *41*, 1820.
(36) Leonard, M.; Hong, H.; Easwar, N.; Strey, H. *Polymer* **2001**, *42*, 5823.